Effect of H-Bonded Liquid Crystal Polymers on CdSe Quantum Dot Alignment within Nanocomposite

Georgy A. Shandryuk,[†] Elena V. Matukhina,[‡] Roman B. Vasil'ev,[§] Alexander Rebrov,[§] Galina N. Bondarenko,[†] Alexey S. Merekalov,[†] Alexander M. Gas'kov,[§] and Raisa V. Talroze*,[†]

A.V. Topchiev Institute of Petrochemical Synthesis, Russian Academy of Sciences, 29 Leninskii prospect, 119912 Moscow, Russia; Moscow State Pedagogical University, 29 Malaya Pirogovskaya, 119882 Moscow, Russia; and Department of Chemistry, M. V. Lomonosov Moscow State University, Leninskie Gory, 119899 Moscow, Russia

Received September 3, 2007; Revised Manuscript Received December 4, 2007

ABSTRACT: Control over nanoparticle shape, liquid crystal (LC) polymer architecture, and the related mesophase structure has made possible the creation of new polymer/CdSe semiconductor nanoparticle composite materials. Surface modification of semiconductor quantum dot nanoparticles by hydrogen-bonded LC polymers resulted in the formation of uniform and coagulation-free bulk systems. The effect of the LC polymer on the alignment of nanoparticles within the composite was established by varying the polymer structure and the size of the quantum dots. The resultant composites represent a new class of nanomaterials in which quantum dots are aligned within the planes provided by the initial smectic layers separated by the periodically located polymer backbones.

Introduction

Over the past decade, the field of nanostructure science and technology has become a broad interdisciplinary area of research.[1−5] Major efforts in this field are directed toward the control and manipulation of the size of nanoparticles, the investigation of material properties (e.g., chemical sensitivity, structural homogeneity, etc.), and the analysis of nanostructure−property relationships. Recent advances in semiconductor nanoparticles known as quantum dots (QDs) have included the preparation of highly monodispersed nanoparticles, the characterization of their structure, and the fabrication of nanoparticle arrays and light-emitting diodes. While the first critical step in utilizing the desirable properties of nanoparticles lies in forming uniform, coagulation-free bulk materials of a diameter smaller than the Bohr exciton, the second crucial step is to incorporate the nanoparticles into a host medium. The ability to combine inorganic nanoparticles and organic molecules into one material is an important aspect of modern materials chemistry.

Numerous attempts have been made to combine the electronic and optical features of nanoparticles with the bulk structure of a polymer medium Polymers, which not only provide exceptional mechanical properties and the ability to form fibers and films, can also enhance the photophysical properties of quantum dots. For instance, in-situ silver(I) reduction allowed control of the reflectivity and surface conductivity of polyimide films metallized with silver.[6,7] A pronounced increase in the band-gap luminescence of cadmium sulfide (CdS) nanocrystals was observed when they were embedded in poly(styrene) and poly(methyl methacrylate).[8] Others have reported that semiconductor quantum dots mixed with polymers provided a higher refractive index than that of the polymers alone.[9] CdS nanoparticles incorporated into poly(*N*-vinylcarbazole) enhanced the photoconductivity of the polymer due to charge generation, transfer, and separation at the interface.[10] CdS quantum dot/SiO_2 nanoparticles were shown to retain the luminescence of the precursor CdS nanoparticles after poly(methyl methacrylate) chains were grown from the surface by controlled/living radical polymerization.[10] It has also been demonstrated that combining quantum dots with poly(*p*-phenylenevinylene) allows direct communication between the nanoparticles and electronically active polymer which shows great promise for creating new electroluminescent materials.[11] Controlling the morphology of electronically active polymer/nanoparticle composites to optimize efficiency of different photoelectronic devices has also been demonstrated.[12]

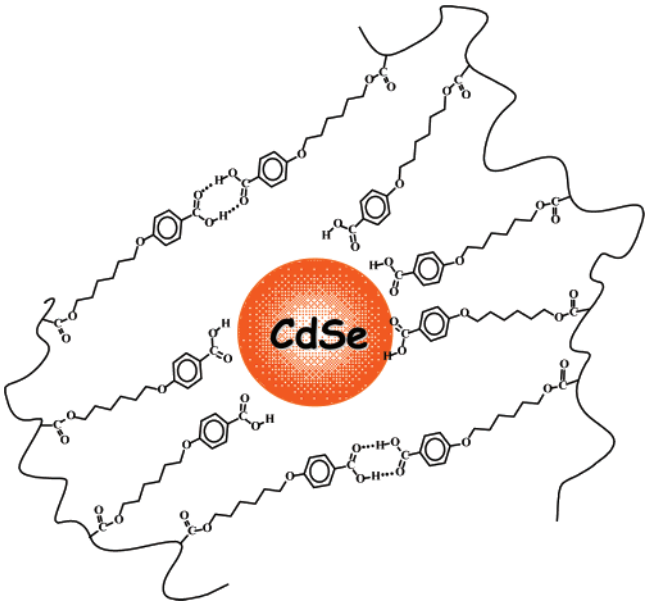

Figure 1. Schematic presentation of the effect of the stabilization of a quantum dot by a side-chain LC polymer.

The next stage in creating new nanocomposite materials could involve the use of anisotropic liquid crystal (LC) systems as the host polymer matrix. Noble metal nanoparticles covered with (or embedded in) a thermotropic low molecular weight LC

[†] Russian Academy of Sciences.
[‡] Moscow State Pedagogical University.
[§] M. V. Lomonosov Moscow State University.

10.1021/ma701983y CCC: $40.75
Published on Web 02/23/2008

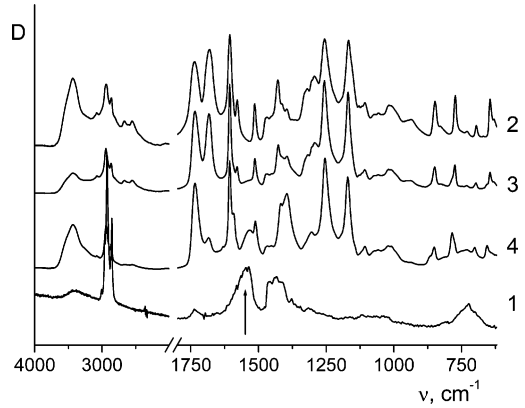

Figure 2. IR spectra of CdSe quantum dots (1), BA-6PA (2), and their blends containing 20 wt % (3) and 40 wt % (4) CdSe quantum dots.

Table 1. Transition Temperatures and the Enthalpy of SmC−Isotropic Transition of BA−*n*PA Polymers and their Composites with CdSe Quantum Dots

composition	T_g, °C	$T_{LC-isotrop}$, °C	ΔH, J/g
BA−6PA	89	169	26.5
BA−6PA + 5% CdSe(2.6 nm)	89	165	21.9
BA−6PA + 10% CdSe(2.6 nm)	89	165.5	20.2
BA−6PA + 20% CdSe(2.6 nm)	90	162	15.8
BA−6PA + 40% CdSe(2.6 nm)	139		
BA−6PA + 10% CdSe(3.2 nm)	91	165.5	18.0
BA−7PA	93	181	30.3
BA−7PA + 5% CdSe(2.4 nm)	98	179	24.3
BA−7PA + 10% CdSe(2.4 nm)	98	176.5	21.1
BA−7PA + 20% CdSe(2.4 nm)	96	172.5	15
BA−7PA + 10% CdSe(3.2 nm)	99	179	21.8
BA−10PA	77	180	27.6
BA−10PA + 5% CdSe(2.4 nm)	83	179	26.7
BA−10PA + 10% CdSe(2.4 nm)	81	177	22.1
BA−10PA + 20% CdSe(2.4 nm)	82	176	18.8
BA−10PA + 10% CdSe(3.2 nm)	81	179	21.8

compound exhibit characteristic LC behavior[13−15] and show that even spherically shaped nanoparticles become optically spheroidal when surrounded by an anisotropic liquid crystal.[16−18]

The anisotropic structure of a LC polymer may provide a way to control the arrangement of inorganic nanoparticles within the matrix. Bliznyuk et al.[19] reported the preferential orientation of single-wall carbon nanotubes in a nematic LC polymer. The first trends in preparation and characterization of LC polymer/nanoparticle composites were published by Barmatov et al.[20−22] The authors found that synthesis the Ag and CdS nanoparticles within a LC copolymer resulted in the formation of nanocomposites accompanied by a strong decrease in the LC temperature range at relatively low loads (<10 wt %). The correct choice of nanoparticle shape, LC polymer architecture, and the related mesophase structure is essential to understanding the distribution and arrangement of the nanoparticles within the LC polymer matrix, the morphology and stability of the composite film, and the material's electronic and optical properties.

The primary goal of this paper is to introduce nanocomposite systems in which a LC polymer matrix controls the loading and alignment of CdSe quantum dots. Side-chain LC polymers of varying spacer length, poly[4-(*n*-acryloyloxyalkoxy)]benzoic acids (BA-*n*PA), having the following chemical structure were used as the host matrixes:

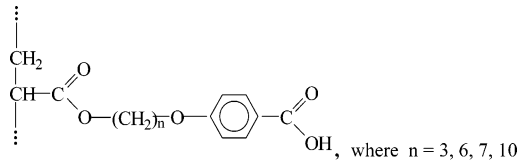

These polymers form the smectic C_A mesophase in the broad temperature range between the glass transition temperature, T_g, and smectic−isotropic transition temperature, T_{Sm-I}.[23,24] The formation of the LC smectic phase in this polymer results from hydrogen bonding (H-bonding) of alkoxybenzoic acid moieties.

This class of polymers was chosen on the basis of the hypothesis that alkoxybenzoic acid moieties in the side polymer chain may substitute the oleic acid molecules but still keep the nanoparticles stabilized.[25] A model depicting this phenomenon is illustrated in Figure 1. If this model proves true, the H-bonded dimers which provide liquid crystallinity should be decoupled, and the stabilized nanoparticles will be arranged within the smectic layers. For this study CdSe quantum dots that were 2.3−3.2 nm in diameter were chosen so as not to exceed the thickness of the smectic layer and disrupt the structure of the polymer composite.

Results and Discussion

The presence of oleic acid during the synthesis of CdSe quantum dots helps to stabilize them in nonpolar solvents. IR spectral analysis of the CdSe sol dried on a KBr surface (Figure 2, spectrum 1) shows several spectral bands: C−H stretching vibrations (2925 cm^{-1}), the CH2 and CH3 scissoring mode (1465 cm^{-1}), the CH3 rocking mode (1380 cm^{-1}), and the CH2 rocking mode (720 cm^{-1}). The intense band at 1540 cm^{-1} (ν_{CO}) indicates the presence of the carboxylate anion, the smaller peak at 1700 cm^{-1} is related to a nonionized form of the carboxylic group, and the small band peaks at approximately 3000 and 1660 cm^{-1} represent the C═C double bond ($\nu_{CH=CH}$). These spectral bands show that oleic acid stabilizes quantum dots in nonpolar solvents through ionic interaction with the surface of the dots. ^1H NMR analysis of the final product indicates the presence of some amount of TOP at the surface though we were not able to make the quantitative calculations. Unfortunately, the majority of oleic acid resonances overlap with signals of TOP. However, as it comes from NMR spectra in addition to oleic acid TOP molecules are also presented on the surface of nanoparticles. In accordance with the quantitative analysis of FTIR data the amount of TOP at the surface does not exceed 25%. At the same time the TGA measurements show that the total amount of organic ligands on the surface of QDs is about 25−30 wt %. The calculations indicate the surface coverage on the 3 nm quantum dots to be 69 ligands (52 oleic acid and 17 TOP molecules) per one quantum dot.

When quantum dots are inserted in BA−*n*PA (Figure 2), the intensities of the spectral bands at 1683, 2550, and 2660 cm^{-1} that are characteristic for the polymer (Figure 2, spectrum 2) decrease (spectra 3 and 4). With the increasing content of QDs one can see the gradual decrease in the intensity of the spectral band at 1683 cm^{-1} that represents C═O bond (ν_{CO}) in the cyclic dimers of the carboxylic groups. Two other bands correspond to the valence vibrations of the OH bond. Simultaneously, new spectral bands at 1540 and 1395 cm^{-1} appear that are related to asymmetric and symmetric CO bond vibrations in COO^- (Figure 2, spectra 3 and 4). The low extinction coefficients of these bands make the intensities much lower than one could expect especially considering the high content of QDs. Interestingly, the IR spectra indicate the presence of just two fragments

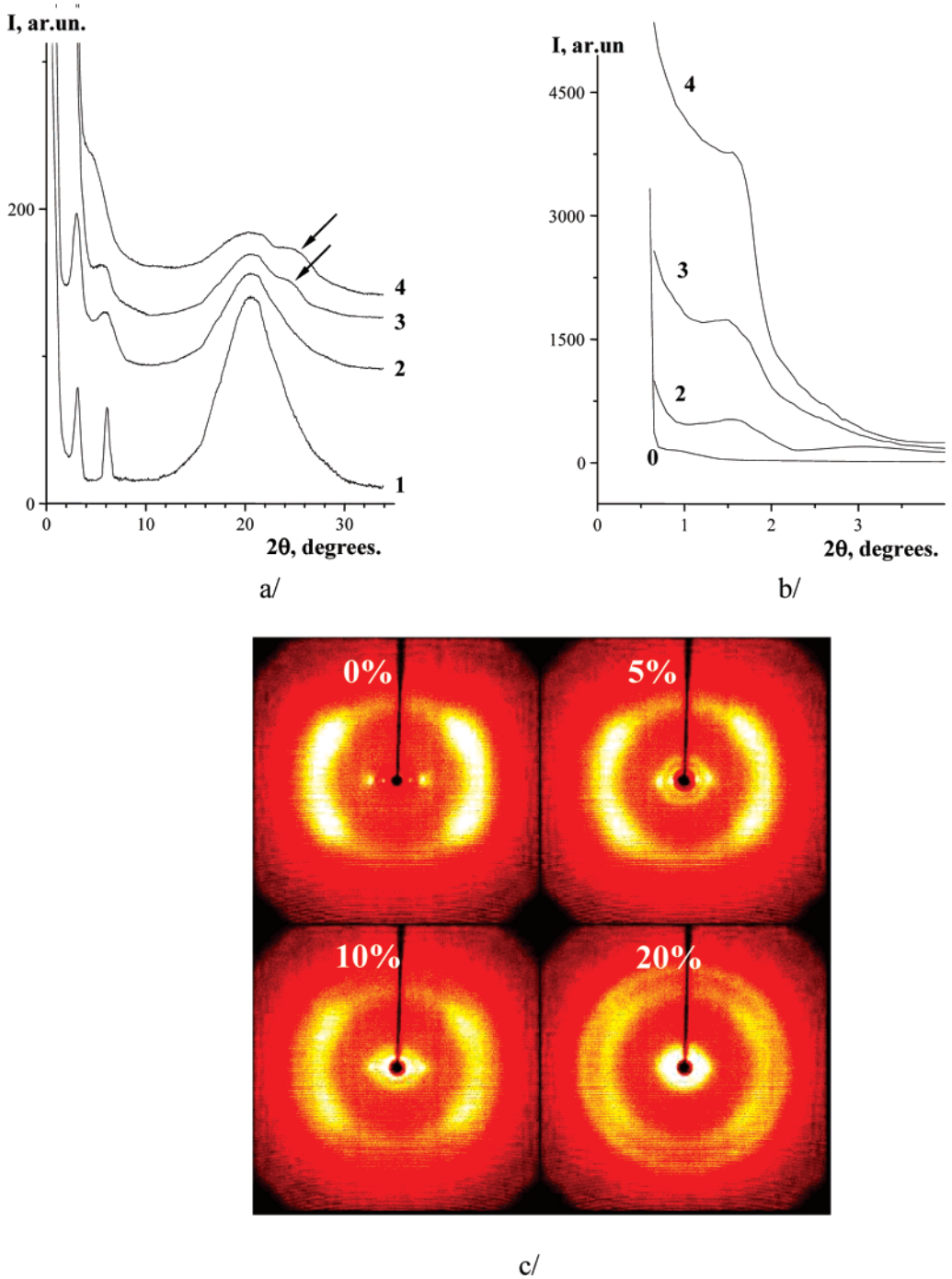

Figure 3. WAXS (a) and SAXS (b) curves and X-ray texture patterns (c) of uniaxially oriented films of BA-6PA (1) and its mixture with 5 (2), 10 (3), and 20 wt % (4) CdSe QDs (2.6 nm). Curve 0: background scattering.

containing carbonyl groups, namely H-bonded carboxylic groups responsible for the formation of mesogenic groups and carboxylate anions appeared due to polymer−quantum dot interactions. There are no signs of free COOH groups.

This means that debonding of the dimer H-bonds during nanocomposite preparation leads to the formation of the carboxylate anions which may only happen as a result of the polymer interaction with quantum dots.

The ionic interaction between the LC polymer and CdSe quantum dots imparts stability to the resulting nanocomposites. Thermal characteristics of the LC polymers and various polymer−quantum dot mixtures are given in Table 1. The liquid crystal−isotropic phase transition temperature drops by 3−10 deg with the incorporation of 20 wt % quantum dots. This is also accompanied by a visible decrease in the transition enthalpy. At the same time the glass transition temperature T_g initially stays stable and then increases as the concentration of quantum dots increases. At 40 wt % quantum dot content, there is no LC−isotropic transition observed, but T_g increased significantly (Table 1).

The IR spectroscopy data and the lack of change in T_g change with the incorporation of 20 wt % or less of quantum dots let us to hypothesize that quantum dots may brake H-bonds and localize within the smectic layers, thus having no influence on the mobility of the backbone segments.

Figure 3 shows the results from XRD. The tilted SmC structure of the BA−*n*PA family of polymers (with the exception of $n = 3$) is characterized by two small-angle peaks ($2\theta \approx 3°$

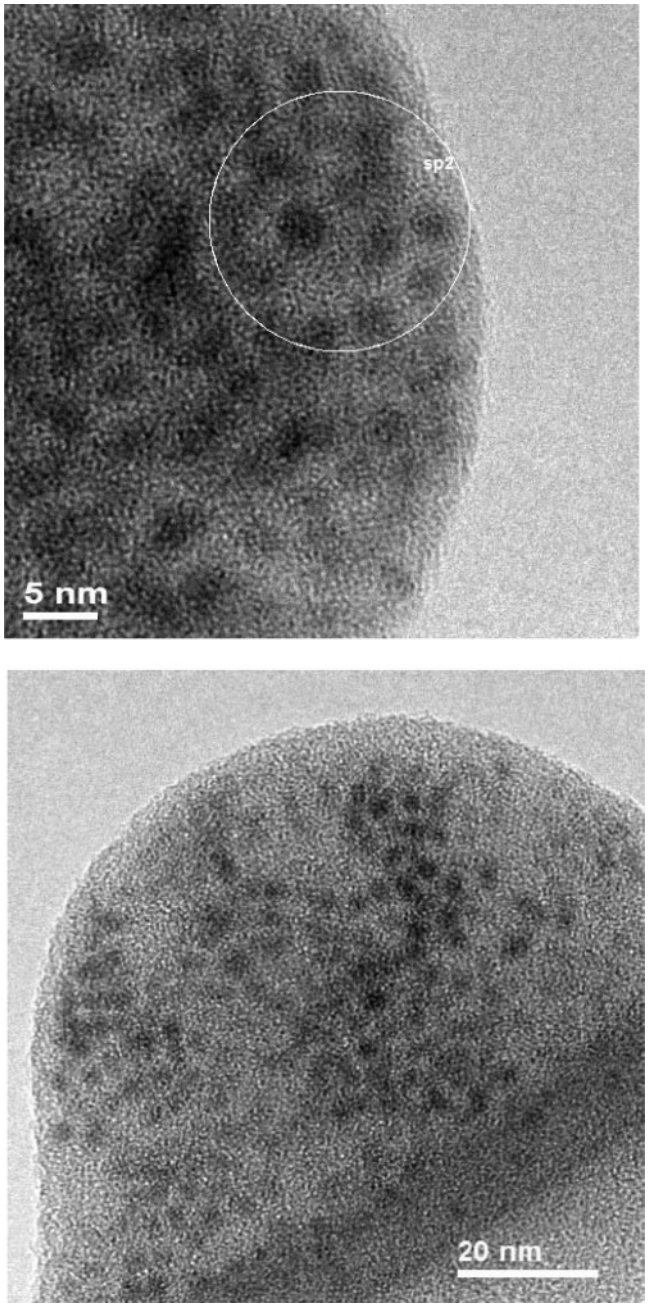

Figure 4. TEM microphotographs of 2.6 nm CdSe−BA−6PA composite containing 20 wt % QDs.

and 6°) related to the first and second reflection orders of the layered packing of H-bonded side groups (Figure 3a, curves 1). Increasing the spacer length (n) for the polymer leds to an increase in the layer periodicity (d) from 2.6 nm ($n = 7$) to 3.2 nm ($n = 10$). Taking into account that the structural layer unit is formed by two side groups of macromolecules,[13] there is no noticeable change in the tilting of the side groups relative to the layer plane. A quite different effect is observed when the spacer is shortened from $n = 7$ down to $n = 6$. In this case there is an increase in the layer periodicity from 2.6 nm ($n = 7$) up to 2.9 ($n = 6$). As has been shown before,[13] changes of this type are the result of a difference in the conformation of the aliphatic spacers and their alignment with respect to both the main chains and the aromatic end groups. In other words, it is caused by the even−odd effect in the flexible spacer.

The XRD patterns drastically change after inserting CdSe quantum dots in the polymer matrix, as illustrated by the XRD

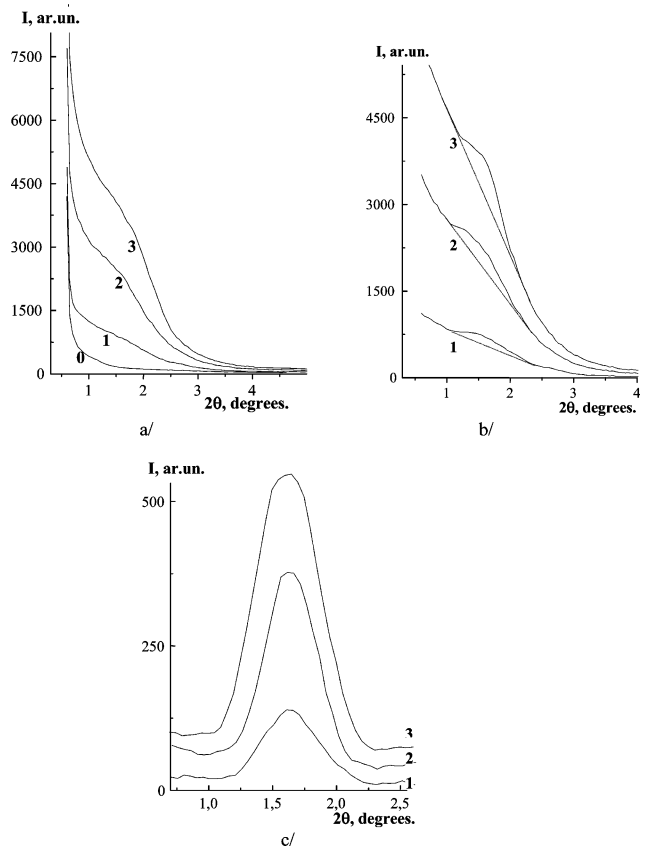

Figure 5. (a) Experimental SAXS curves of BA−10PA composites with 5 (1), 10 (2), and 20 wt % (3) 2.4 nm CdSe QDs. (b) Same curves after subtracting the background curve (0). (c) Same curves after subtracting the background and the exponential curve.

curves of BA−6PA and its composites with 2.6 nm QDs given in Figure 3. Comparison of diffraction curves of the polymer (1) with those of its composites (2−4) shows that the amorphous halo in the angular region $2\theta = 13°-30°$ (Figure 3a) related to the scattering on the side chains of the macromolecules does not shift. However, a well-defined, but broad ($\Delta_{1/2} \sim 3.1°$) maximum at $2\theta = 25.4°$ appears in the form of a shoulder on the amorphous halo. This peak may be attributed to the (111) reflection of the cubic crystalline structure of CdSe previously predicted for nanoparticles.[26−28] Note that the half-width ($(\Delta_{1/2} = 3.14°$) of the (111) reflection is in a good coincidence with the size of the inserted nanoparticles as calculated in accordance with the Sherrer formula.[29] As for the scattering at small angles, it is clear that a substantial rise in the scattering intensity at small angles resulted from the incorporation of the CdSe particles (Figure 3b,c).

There are four condensed wide-angle maxima (Figure 3c) with an azimuthal position that does not change with the insertion of QDs up to 20 wt %. These maxima being related with the scattering on to the tilted side groups of the matrix polymer with SmC structure correspond to the tilt of side groups in the SmC structure of the matrix polymer,[23,24] which seem to be present in the composites even at high CdSe quantum dot content. As for the maxima at $2\theta \approx 3°$ and 6° connected with responsible for the layered structure, both register at similar polymer angle positions in the WAXS diagram (Figure 3a) and textured X-ray pattern (Figure 3c) when the quantum dot content is 5 wt %. However, the relative intensities of these maxima for the pure polymer and the composite are different: for the latter the intensity of the first maximum becomes higher than that of the second maximum. As the amount of QDs is increased

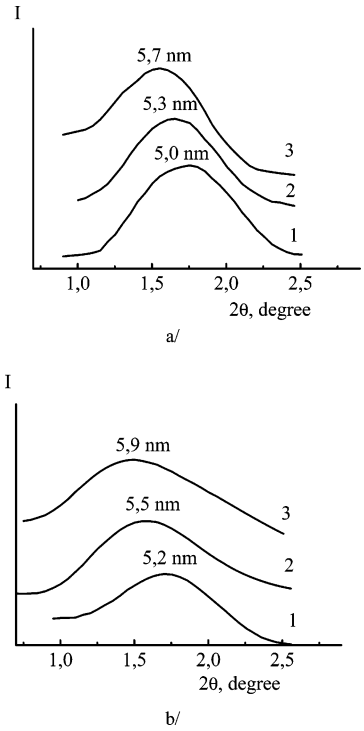

Figure 6. Shift in the angle position of the SAXS reflections for BA−*n*PA composites with different spacer group lengths [$n = 3$ (1), 7 (2), and 10 (3)] and a quantum dot size fixed at 2.4 nm (a) and for BA−7PA composites (b) with CdSe dots of different sizes [2.4 nm (1), 2.7 nm (2), 3.2 nm (3)].

up to 10−20 wt %, the first maximum becomes screened by the intensive SAX scattering from by the QDs whereas the second one is shifted down to smaller angles. Another point of interest is that there is no noticeable aggregation of quantum dots even at high contents, as illustrated in the TEM microphotograph of the nanocomposite containing 20 wt % QDs (Figure 4).

The experimental X-ray diffraction curves of BA−10PA composites containing different amounts of 2.4 nm CdSe quantum dots are presented in Figure 5a. At wider angles the original curves (1−4) are in agreement with the background curve (0). After subtracting of the background curve (0), one can see the small-angle maxima becomes more readily apparent (Figure 5b). The above curves are, in part, well approximated by the exponents as indicated with the dotted lines. Subtraction of the exponential curves allows isolation of the well-defined maxima in the small-angle scattering curves (Figure 5c). An increase in the number of the quantum dots in the unit volume appropriately leads to an increase in the integral intensity of the small-angle maximum, but its angular position does not change.

The properties of the small-angle maxima are related to the layered structure of the nanocomposites. Consider when nanocomposites made of polymers with different spacer lengths, BA−6PA, BA−7PA, and BA−10PA, are mixed with the equal amounts of 2.4 nm CdSe particles. One can see the gradual increase in the layer thickness associated with the increasing spacer length (Figure 6a). The calculated difference between the interlayer periodicity of the composite systems and matrix polymers shows that it is equal to the diameter of the quantum dot. This tendency is also manifested if the size of the quantum dot is increased while the spacer length stays constant (Figure 6b). Moreover, an azimuth scanning of XRD patterns obtained for oriented samples (Figure 7) shows that the small-angle maximum is localized at the equator, just as it is for the initial polymer matrix.

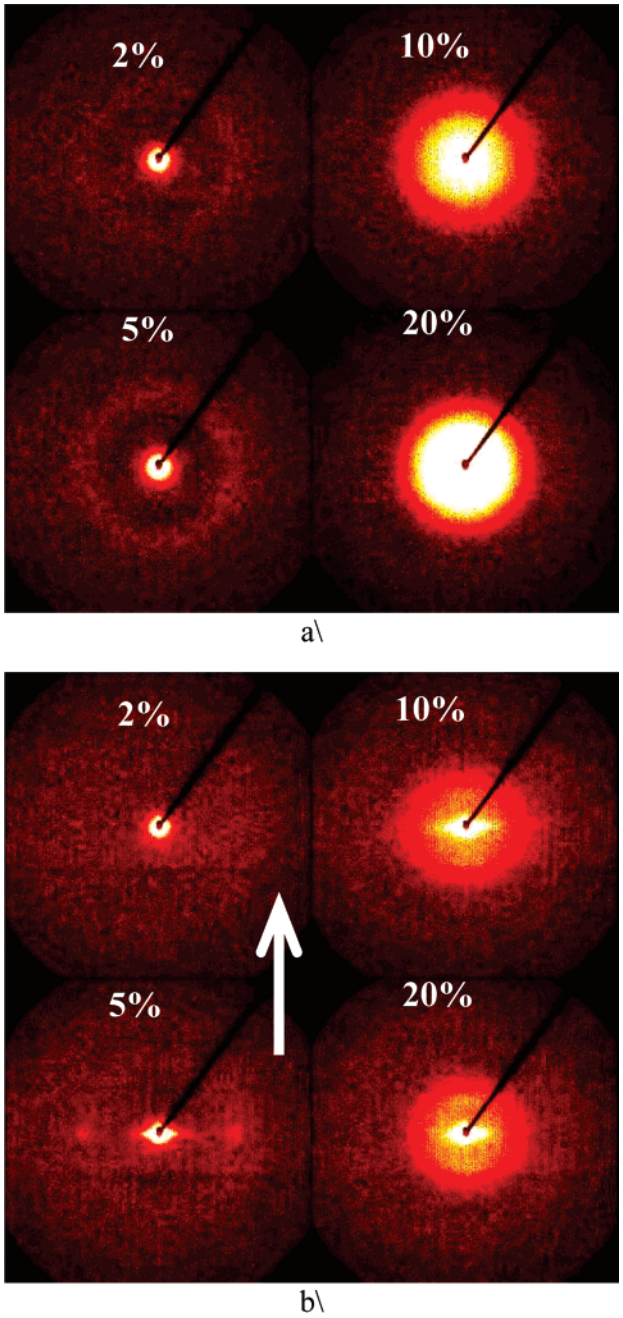

Figure 7. SAXS patterns of BA−6PA composites with 0, 5, 10, and 20 wt % 2.6 nm CdSe QDs before (a) and after (b) 100% stretching (an arrow indicates the orientation direction).

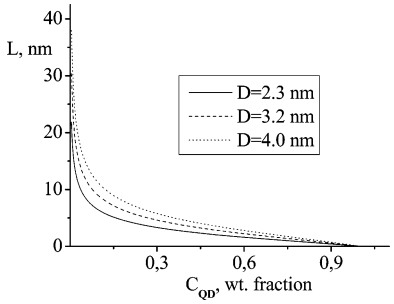

Figure 8. Theoretical curves depicting the relationship between the interparticle distance in the nanocomposite's bulk and their content.

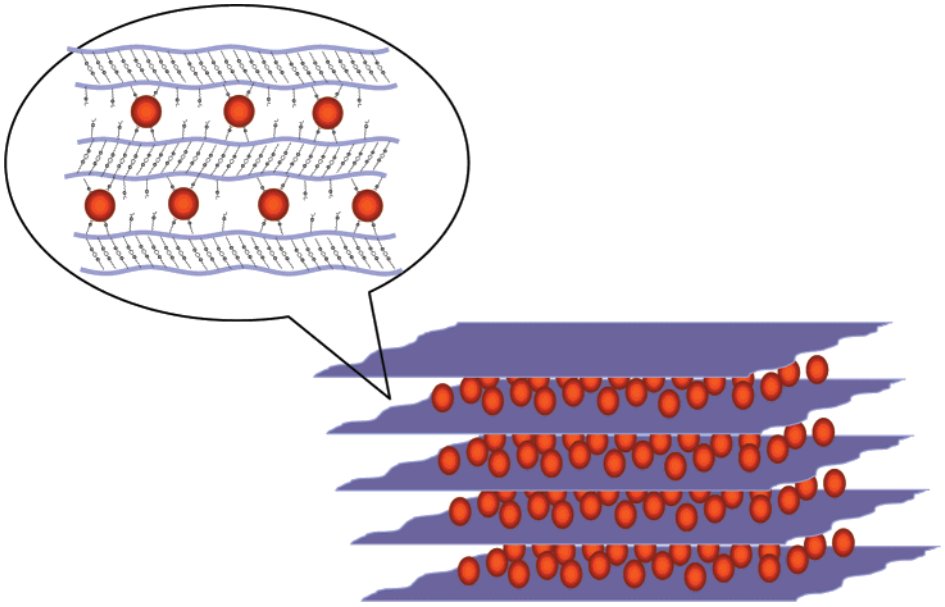

Figure 9. Schematic representation of the structure of CdSe/BA−*n*PA nanocomposite.

Taken together, these X-ray data and the DSC and IR data noted above also demonstrate that the intralayer location of the quantum dots makes the layer thickness larger than that of the matrix polymers. In addition, when the quantum dots are added, the scattering shape in the small angular region for isotropic and oriented stretched samples (Figure 7) changes from a spherical (a) to an ellipsoidal one (b). It happens in contrast to the fact that the spherical shape of the dots cannot be changed under stretching. There is no visible aggregation of the quantum dots (Figure 4) at the contents used, and the tilt angle of side chains undergoes no change upon stretching (Figure 3). Taking into account that the shape of the scattering in the small-angular region is determined by the shape of a scatter,[29] there is good reason to believe that the transformation of the scattering shape presented in Figure 7 is connected with the preferred alignment of the spherical CdSe particles. Particle organization follows in accordance with regulations confirmed for LC polymers[23,24] and is due to noncovalent bonding of the quantum dots with the LC polymer matrix. The latter controls the preferable alignment of quantum dots along the stretching axis parallel to the smectic planes.

The strong rise in the intensity of SAXS with increasing content of QDs seen in Figures 3 and 7 shows that the scattering from individual particle proceeds in a correlative manner. This means that even at 10−20 wt % the quantum dots should be located close to each other. To resolve this issue, the average distance (L) between QDs was calculated (eq 6). Figure 8 presents the curves for the distance as a function of the QD concentration and size. This distance dropped sharply as the concentration of QDs reached 10 wt % and then decreased more slowly, indicating closer packing of the nanoparticles at contents above 10−20 wt %. Taking into account that the L values shown in Figure 8 correspond to an approximation of the upper distance limit that is obtained in a "homogeneous distribution", one may expect that "in-layer" packing of QDs should result in distances even smaller than the ones given in Figure 8.

A schematic representation of the BA−*n*PA/quantum dot nanocomposite is given in Figure 9. The ideal picture reflects the formation of QDs layers separated from the polymer layer on the regular bases. The calculated values of L at 40 wt % content of QDs are equal to approximately 1−2 diameters of nanoparticles. This corresponds to their dense packing in the layers when most of H-bond dimers are disconnected, which is proved by IR spectra (Figure 2) that show the strong drop in the intensity of ν_{CO} at 1683 cm^{-1}. Moreover, the thermal properties of the composite change when the content of QDs reaches 40 wt %. The polymer LC phase disappears after being substituted by the polymer−QD layered structure, and as illustrated earlier in Table 1, the change in T_g reflects a thermal transition that is governed by interactions between the polymer and the QDs. It is obvious that the concentration at which such a transition takes place will primarily depend on the size of the QDs. Moreover, the calculations also show that the polymer matrix may be filled in with a high amount of QDs with no significant aggregation.

Conclusion

The formation of organized nanocomposites based on CdSe quantum dots and LC polymers is described in this paper. The breaking of H dimers and the interaction of the polymer carboxylic groups with the QD's surface govern the localization of QDs and result in the formation of polymer nanolayers separated by QD nanolayers. SAXS studies were essential for quantifying the thickness of the nanolayers and the contribution of the polymer spacer length, the QD size, and the QD content to the structure of the nanolayers and the resulting nanocomposite.

Experimental Section

LC Polymer Synthesis. Monomers, 4-(*n*-acryloyloxyalkoxy)-benzoic acids (BA−*n*A), were synthesized as previously described[30] and then polymerized in benzene at 63 °C for 75 h to form the polymer, BA−*n*PA. 2,2′-Azobis(isobutyronitrile) (0.1% of the total weight of the monomer) was used as the initiator. Polymers were precipitated from the benzene solution, then separated, dissolved in tetrahydrofuran (THF), reprecipitated with benzene, and dried overnight under vacuum. The polymers yield was 80−90%.

Nanoparticle Synthesis. Cd Se nanoparticles were synthesized in accordance with the procedure used by Vasiliev et al.[26] Cadmium acetate (0.5 mmol), $Cd(CH_3COO)_2 \cdot 2H_2O$, and oleic acid (2 mmol), $CH_3(CH_2)_7CH{=}CH(CH_2)_7COOH$, were dissolved in 5 mL of diphenyl ether. The reaction was carried out at 140 °C for 1 h under argon flow to remove water and acetic acid. Maintaining the temperature between 130 and 200 °C, 0.5 mL of 1 M solution of

selenium trioctylphosphine in trioctylphosphine was added while stirring. Nanoparticles began to grow after 5 min, and by adjusting the temperature, their size could be controlled. When the reaction was complete, the mixture was cooled to room temperature, and a volume of acetone equal to the solution volume was added to precipitate the quantum dots. The coagulated quantum dots were then centrifuged, washed twice with acetone, and dissolved in an applicable solvent.

Polymer/Nanoparticle Composite Synthesis. A special procedure for the preparation of polymer−quantum dot blends was developed for this study. CdSe solution (10 mg/mL) was added dropwise to 50 mg/mL of the BA−*n*PA polymer solution while stirring at room temperature. After stirring 15−20 min, the colored solution was added to a 3× volume of hexane to precipitate the polymer−quantum dot composite. The solid precipitate was washed with hexane and then dried overnight under vacuum at room temperature. The resulting colored powder was used for film preparations in further studies.

Characterization of Polymers. SEC **(**size exclusion chromatography) analysis was conducted on a Waters Breeze 1515 series liquid chromatograph equipped with a dual absorbance detector (Waters 2487), manual injector, and three styrogel columns (HR1, HR3, HR4) using linear polystyrene standards for calibration and tetrahydrofuran (THF) as the mobile phase. The molecular weights of the polymers were found to be $M_w = (3.2-7.7) \times 10^4$ Da. The variability in M_w is related to the different polymers ($n = 3-10$). The polydispersity index did not exceed 1.5−1.7.

Characterization of Composites. The thermal properties of the blends were investigated using differential scanning calorimeter (Mettler TA-4000) equipped with a DSC-30 heating cell (Mettler Toledo, Switzerland) at a heating rate of 10 K/min under argon. Optical observations were made using a polarizing microscope Polam L-213 (LOMO, St. Petersburg, Russia) equipped with a Mettler Toledo FP-82 HT hot stage and a microprocessor temperature control unit. The temperature of the tested samples was maintained with an accuracy of up to 0.1 °C.

The powder X-ray diffraction (XRD) patterns were collected on a DRON-3M (Burevestnik, St. Petersburg, Russia) X-ray diffractometer (Cu Kα radiation, Ni-filtered, transmission mode), equipped with an antibackground slit covered the small angular region up to $2\theta = 0.5°$. The diffractometer was calibrated in wide and small angular regions using α-Al_2O_3 and silver behenate with known crystal diffractions. Wide-angle (WAXS) and small-angle (SAXS) X-ray scattering analyses of oriented samples were performed using a 12 kW Rigaku rotating anode generator (Rigaku, Japan) equipped with a GADDS 2D-area detector and a flat graphite monochromator (Cu Kα irradiation, $\lambda = 1.54$ nm) (Bruker AXS, Germany). The angle positions 2θ and half-widths of the Bragg reflections were measured using the EVA-Diffrac-Plus software package (Bruker AXS, Germany).

IR spectra were recorded with IFS 66v/s (Bruker, Germany). Samples were prepared as either thin solid films cast from solutions and placed on KBr or as a powder blended with KBr. To make the quantitative estimation of the amount of different ligands at the quantum dot's surface, we have used FTIR spectroscopy. The ratio (K) between the extinction coefficients of the spectral band at 1378 cm^{-1} related to C−H bond vibration in CH_3 group and the complex spectral band at 1464 cm^{-1} attributed to C−H vibration in CH_3 and CH_2 groups is known to be a characteristic feature for every individual hydrocarbon fragment if the number of C atoms is more than 6.[31] The average K value measured within the spectrum of the oleic acid is 0.1, whereas for the TOP this ratio is 0.317. If we assume that the only ligands for nanoparticles may be either oleic acid or TOP or both and take into account the ratio values K measured for oleic acid (0,1) and TOP (0.317) calculated from the experimental data, K_{total} is

$$K_{total} = xK_{oleic\ acid} + (1 - x)K_{TOP}$$

In accordance with the above equation, the content of TOP on the surface was varied in the range between 10 and 25%.

Thermogravimetry analysis (TGA) was carried out with Pyris 1 TGA (Perkin-Elmer).

Calculations. 1. The surface coverage on quantum dots was estimated by means of TGA data that indicated the total amount of the organic residues on QDs to be of about 30 wt %. Taking into account the density of CdSe QDs to be equal to 5.81 g/cm^3, the volume of the 3 nm QD and its weight were calculated as 1.4×10^{-20} cm^3 and 8.1×10^{-20} g, respectively. With the assumption that the content of ligands on the surface is distributed as 25 mol % TOP and 75 mol % oleic acid, the resultant number of ligand molecules is about 69 (52 molecules of oleic acid and 17 molecules of TOP).

2. The average distance between two quantum dots located in the polymer matrix was calculated with the assumption that they are homogeneously distributed within the volume.

The mass fraction of quantum dots (C_{QD}) may be presented by the following equation

$$C_{QD} = M_{QD}/(M_{QD} + M_P) \tag{1}$$

where M_{QD} and M_P are total mass of quantum dots and of polymer, respectively.

The total mass of quantum dots is given by

$$M_{QD} = N_{QD}\rho_1 v_1 \tag{2}$$

where N_{QD} is the number of quantum dots, ρ_1 the density of quantum dots, and v_1 the volume of a single quantum dot.

The total volume of the composite as a whole (V) may be given by the following equation

$$V = V_p + N_{QD}v_1 = M_P/\rho_2 + M_{QD}/\rho_1 \tag{3}$$

where V is the total volume of a composite, V_p the polymer volume, and ρ_2 the polymer density.

The number of the quantum dots per volume unit is given as

$$\frac{N_{QD}}{V} = \frac{M_{QD}}{\rho_1 v_1\left(\frac{M_P}{\rho_2} + \frac{M_{QD}}{\rho_1}\right)} = \frac{1}{\rho_1 v_1\left(\left(\frac{1}{C_{QD}} - 1\right)\frac{1}{\rho_2} + \frac{1}{\rho_1}\right)} \tag{4}$$

From eq 4 an "effective" volume per one quantum dot (v) is calculated as

$$v = v_1\left(1 + \frac{\rho_1}{\rho_2}\left(\frac{1}{C_{QD}} - 1\right)\right) \tag{5}$$

For particles having spherical shape the average distance (L) between the neighboring QDs will depend on the QDs's diameter (D) and can be calculated with eq 6:

$$L = D\left(1 + \alpha\frac{1 - C_{QD}}{C_{QD}}\right)^{1/3} - D \tag{6}$$

where $\alpha = \rho_1/\rho_2$.

Acknowledgment. We gratefully acknowledge financial support from the Russian Federal Agency for Science and Innovations (project no. 02.513.11.3022), the 8th Program of the Presidium of Russian Academy of Sciences (RAS), and the 4th Program of the Division of Chemistry and Materials Science of RAS. The authors are grateful to Dr. Elena Suvorova-Buffat (Institute of Crystallography, RAS) for TEM studies and Dr. Esi Ghartey-Tagoe (Corium International Inc.) for the fruitful discussions.

References and Notes

(1) Alivisatos, A. P. *Science* **1996**, *271*, 933.
(2) Alivisatos, A. P. *J. Phys. Chem.* **1996**, *100*, 13226.

(3) Murray, C. B.; Norris, D. J.; Bawendi, M. G. *J. Am. Chem. Soc.* **1993**, *115*, 8705.
(4) Li, J. J.; Wang, A.; Guo, W.; Keay, J. C.; Mishima, T. D.; Johnson, M. B.; Peng, X. *J. Am. Chem. Soc.* **2003**, *125*, 12567.
(5) Parak, W. J.; Manna, L.; Simmel, F. C.; Gerion, D.; Alivisatos, A. P. *Nanoparticles* **2004**, 4.
(6) Southward, R. E.; Thompson, D. W.; St. Clair, A. K. *Chem. Mater.* **1997**, *9*, 501.
(7) Southward, R. E.; Thompson, D. S.; Thompson, D. W.; St. Clair, A. K. *Chem. Mater.* **1997**, *9*, 1691.
(8) Tamborra, M.; Striccoli, M.; Comparelli, R.; Curri, M.; Petrella, A.; Agostiano, A. *Nanotechnology* **2004**, *15*, S240.
(9) Caseri, W. *Macromol. Rapid Commun.* **2000**, *21*, 705.
(10) Chen, W.; Joly, A. G.; Malm, J. O.; Bovin, J. O.; Wang, S. *J. Phys. Chem. B* **2003**, *107*, 6544.
(11) Farmer, S. C.; Patten, T. E. *Chem. Mater.* **2001**, *13*, 3920.
(12) Skaff, H.; Emrick, T. J. *J. Am. Chem. Soc.* **2004**, *126*, 11322.
(13) Dabbousi, B. O.; Bawendi, M. G.; Onitsuka, O.; Rubner, M. F. *Appl. Phys. Lett.* **1995**, *66*, 1316.
(14) Tessler, N.; Medvedev, V.; Kazes, M.; Kan, S.; Banin, U. *Science* **2002**, *295*, 1506.
(15) Liu, J.; Tanaka, T.; Sivula, K.; Alivisatos, A. P.; Frechet, J. M. J. *J. Am. Chem. Soc.* **2004**, *126*, 6550.
(16) Kanayama, N.; Tsutsumi, O.; Kanazawa, A.; Ikeda, T. *Chem. Commun.* **2001**, 2640.
(17) Mitov, M.; Portet, C.; Bourgerette, Ch.; Snoeck, E.; Verelest, M. *Nat. Mater.* **2002**, *1*, 229.
(18) Mueller, J.; Soennichsen, C.; von Poshinger, H.; von Plessen, H.; Klar, T. A.; Feldmann, J. *Appl. Phys. Lett.* **2002**, *81*, 171.
(19) Bliznyuk, V. N.; Singamaneni, S.; Sanford, R. L.; Chiappetta, D.; Crooker, B.; Shibaev, P. V. *J. Nanosci. Nanotechnol.* **2005**, *5*, 1651.
(20) Barmatov, E. B.; Pebalk, D. A.; Barmatova, M. V. *Langmuir* **2004**, *20*, 10868.
(21) Barmatov, E. B.; Medvedev, A. S.; Pebalk, D. A.; Barmatova, M. V.; Nikanorova, N. I.; Zezin, S. B.; Shibaev, V. P. *Polym. Sci.* **2006**, *A48*, 665.
(22) Barmatov, E. B.; Pebalk, D. A.; Barmatova, M. V. *Polym. Sci.* **2007**, *B49*, 47.
(23) Merekalov, A. S.; Kuptsov, S. A.; Shandryuk, G. A.; Bezborodov, V. S.; Terentjev, E. M.; Talroze, R. V. *Liq. Cryst.* **2001**, *28*, 495.
(24) Shatalova, A. M.; Shandryuk, G. A.; Bondarenko, G. N.; Kuptsov, S. A.; Talroze, R. V.; Plate', N. A. *Polym. Sci.* **2003**, *45*, 245.
(25) Shandryuk, G. A.; Rebrov, A. V.; Vasil'ev, R. B.; Dorofeev, S. G.; Merekalov, A. S.; Gas'kov, A. M.; Talroze, R. V. *Polym. Sci.* **2005**, *47*, 1241.
(26) Vasiliev, R. B.; Dorofeev, S. G.; Dirin, D. N.; Belov, D. A.; Kuznetsova, T. A. *Mendeleev Commun.* **2004**, *14*, 169.
(27) Talapin, D. V.; Rogach, A. L.; Mekis, I.; Haubold, A.; Kornowski, A.; Weller, H. *Colloids Surf., A* **2002**, *202*, 145.
(28) Rockenberger, J.; Troeger, I.; Kornowski, A.; Vossmeyer, T.; Eychmueller, A. J.; Feldhaus Weller, H. *J. Phys. Chem. B* **1997**, *101*, 269.
(29) Guinier, A. *Théorie et technique de la radiocristallographie*, 2nd ed.; DUNOD: Paris, 1956.
(30) Portugall, M.; Ringsdorf, H.; Zentel, R. *Makromol. Chem.* **1982**, *B183*, 2311.
(31) Belamy, L. J. *The Infra-red Spectra of Complex Molecules*; John Wiley & Sons: New York, 1962; 580 pp.

MA701983Y